EEET ECOLOGICAL ENGINEERING & ENVIRONMENTAL TECHNOLOGY

Ecological Engineering & Environmental Technology, 2026, 27(8), 345–359
https://doi.org/10.12912/27197050/225418
ISSN 2719–7050, License CC-BY 4.0

Received: 2026.06.30
Accepted: 2026.07.10
Published: 2026.08.01

Spatio-temporal assessment of Atlas cedar decline and vegetation-drought dynamics: Belezma National Park (Algeria), 1985–2025

Salah Boukhalfa[1*], Ahmed Bougherara[2]

[1] Teacher Education College of Setif, Messaoud Zeghar, University of Setif 2, 19000 Setif, Algeria
[2] Faculty of Earth Sciences, Geography and Urban Planning, University of Constantine 1 – Brothers Mentouri, Constantine, Algeria
* Corresponding author's e-mail: salahboukhalfa5@gmail.com

ABSTRACT

Atlas cedar (*Cedrus atlantica*) forests in the Aurès massif of eastern Algeria have been declining for decades, but the relative weight of climatic and non-climatic drivers remains debated. We reconstructed land-cover and vegetation–drought dynamics for Belezma National Park over 1985–2025 using Landsat surface reflectance processed in Google Earth Engine, Random Forest classification of five land-cover classes at decadal steps, per-pixel Theil–Sen and Mann–Kendall trend analysis of spectral indices, and TerraClimate-derived SPEI. Classification accuracy was high (overall accuracy 0.971–0.998; kappa 0.962–0.997). The cedar class contracted from 1561 to 720 ha (−53.9%), while mixed forest expanded by 93.4%. Park-mean NDVI rose significantly even as growing-season SPEI and PDSI declined, and annual NDVI was uncorrelated with SPEI ($r = 0.09$, $p = 0.58$), indicating that aggregate greening masks a localised, drought- and disturbance-associated loss of cedar.

Keywords: Atlas cedar, land-cover change, SPEI, Landsat, Aurès, Algeria.

INTRODUCTION

The Atlas cedar (*Cedrus atlantica* (Endl.) Manetti ex Carrière) anchors the highest-elevation forests of the Maghreb and is one of the few conifers able to form closed stands on the semi-arid mountains of North Africa. In the Aurès massif of eastern Algeria the species has long been recognised as both a biogeographical relict and a management priority (Abdessemed, 1981; Bentouati, 2008), and it is now listed among the world's threatened conifers (*Cedrus atlantica* – Threatened Conifers of the World). Palaeoecological reconstructions show that the species has persisted in these mountains through the Holocene while contracting repeatedly during dry phases (Alba-Sánchez et al., 2025a, 2025b), and species-distribution models project further range loss under continued warming (Bouahmed et al., 2019; Laala and Adimi, 2024). Repeated waves of crown thinning, branch mortality and stand-level dieback have been documented across the Aurès since at least the 1980s (Bentouati and Bariteau, 2006; Kherchouche et al., 2012), with the most severe episode following the prolonged drought of the late 1990s and early 2000s.

Why the cedar is dying is less settled than the fact that it is. Dendrochronological work points to a climate shift toward warmer and drier growing seasons as the dominant long-term pressure (Sarmoum et al., 2019), a reading consistent with the increased frequency of Mediterranean drought (Hoerling et al., 2012) and with multi-century reconstructions that place recent decades among the driest in northwestern Africa (Touchan et al., 2011; Cook et al., 2016). Studies in the Moroccan Middle Atlas reach a similar conclusion, linking decline to rising drought sensitivity, particularly in older trees (Linares et al., 2011; Linares et al., 2013), and tree-ring precipitation

reconstructions from Algerian cedar stands document a long history of moisture limitation (Slimani et al., 2021). Against this climatic backdrop, biotic and anthropogenic agents are reported to act as accelerants: outbreaks of bark beetles and wood-boring insects have been identified as a potent proximate driver of cedar mortality in the Aurès (Beghami et al., 2020), and the arthropod communities of Belezma itself are now being catalogued in detail (Zereg et al., 2025). Grazing pressure, fuelwood cutting and fire complete the list of disturbances that a national park is meant to contain but rarely eliminates.

Satellite remote sensing offers the only practical way to place these processes in a consistent spatial and temporal frame. Earlier Landsat-based assessments in the Aurès and at Belezma have mapped cover change and cedar retreat over multi-decadal windows (Belloula and Beghami, 2018; Ait Medjber et al., 2024), and the broader literature on dendrochronology and remote sensing in North Africa has matured rapidly (Esper et al., 2024). What has been harder to establish is whether the vegetation signal that a park-scale sensor records actually tracks the climatic drought signal, or whether the two diverge, which would imply that drivers other than rainfall deficit govern the changes on the ground.

This study addresses that question for Belezma National Park over a forty-year window. We had three aims: to quantify land-cover change between 1985 and 2025 with an explicit accuracy assessment; to characterise per-pixel trends in vegetation and moisture indices alongside trends in precipitation, temperature and drought indices; and to test directly whether interannual vegetation activity is coupled to the Standardized Precipitation Evapotranspiration Index (SPEI). The results bear on how managers should read greenness data for a park whose flagship species occupies a small and shrinking fraction of its area.

STUDY AREA

Belezma National Park lies on the north-western shoulder of the Aurès massif in Batna Province, eastern Algeria, immediately west of the city of Batna (Figure 1). The park covers roughly 26,000–28,000 ha of mountain terrain rising from semi-arid piedmont to summits above 2.000 m (the elevation model spans about 871–2.127 m), and it protects one of the three main Algerian cedar massifs alongside the Aurès *sensu stricto* and the Belezma–Aurès chain described in the foundational phytosociological survey of the area (Abdessemed 1981). The climate is Mediterranean with a strong continental and semi-arid character: hot dry summers, cold winters, and a marked interannual variability in cool-season rainfall that propagates directly into

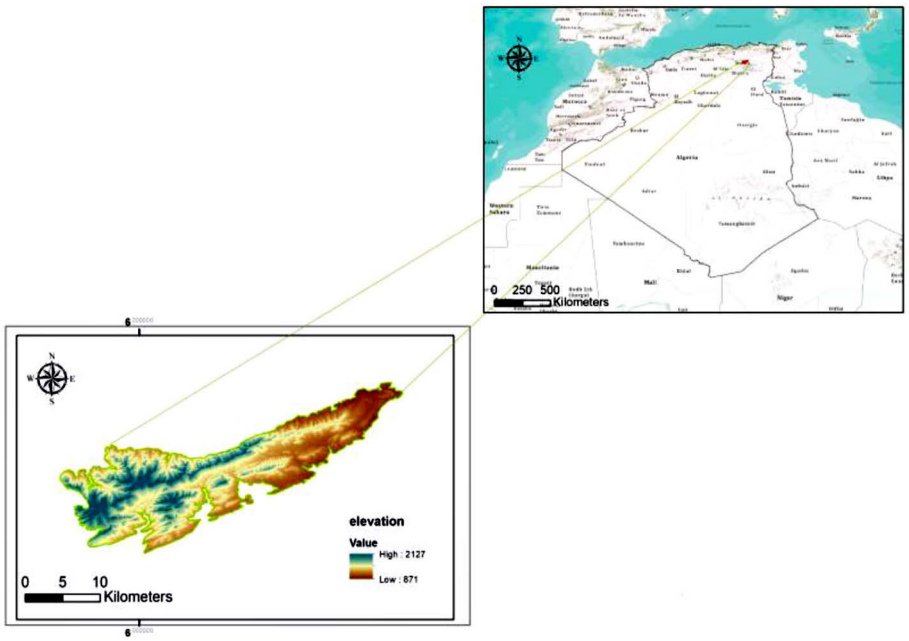

Figure 1. Study area: Belezma National Park in north-eastern Algeria (locator, top right) and its elevation model (871–2.127 m), Batna Province, Aurès massif

growing-season moisture availability. Vegetation is organised along the elevation and exposure gradient. Atlas cedar occupies the cooler, more humid upper slopes and north-facing aspects, frequently in mixture with holm oak and other broadleaves; below and around it lie degraded matorral, shrub-steppe and rangeland, cultivated pockets on gentler ground, and bare or sparsely vegetated soils on eroded and south-facing slopes. The cedar stands here are the subject of a long record of decline and conservation concern (Bentouati and Bariteau, 2006; Bentouati, 2008), which makes the park a natural laboratory for separating climatic from non-climatic drivers of forest change. Independent field photographs taken within the park in 2015 document the condition of the cedar stands and are used here as ground verification of the mapped decline.

MATERIALS AND METHODS

Satellite data and preprocessing

The complete analytical workflow is summarised in Figure 2. All optical processing was carried out in Google Earth Engine (Gorelick et al., 2017). We used Landsat 5 Thematic Mapper for the earlier epochs and Landsat 8/9 Operational Land Imager for the recent ones, drawing on the USGS surface-reflectance products. Landsat 7 ETM+ was deliberately excluded to avoid the scan-line corrector (SLC-off) gaps that affect imagery after 2003. For each target year we masked clouds and cloud shadows using the scene quality-assessment bands and compiled growing-season median composites, which suppress residual cloud and phenological noise while

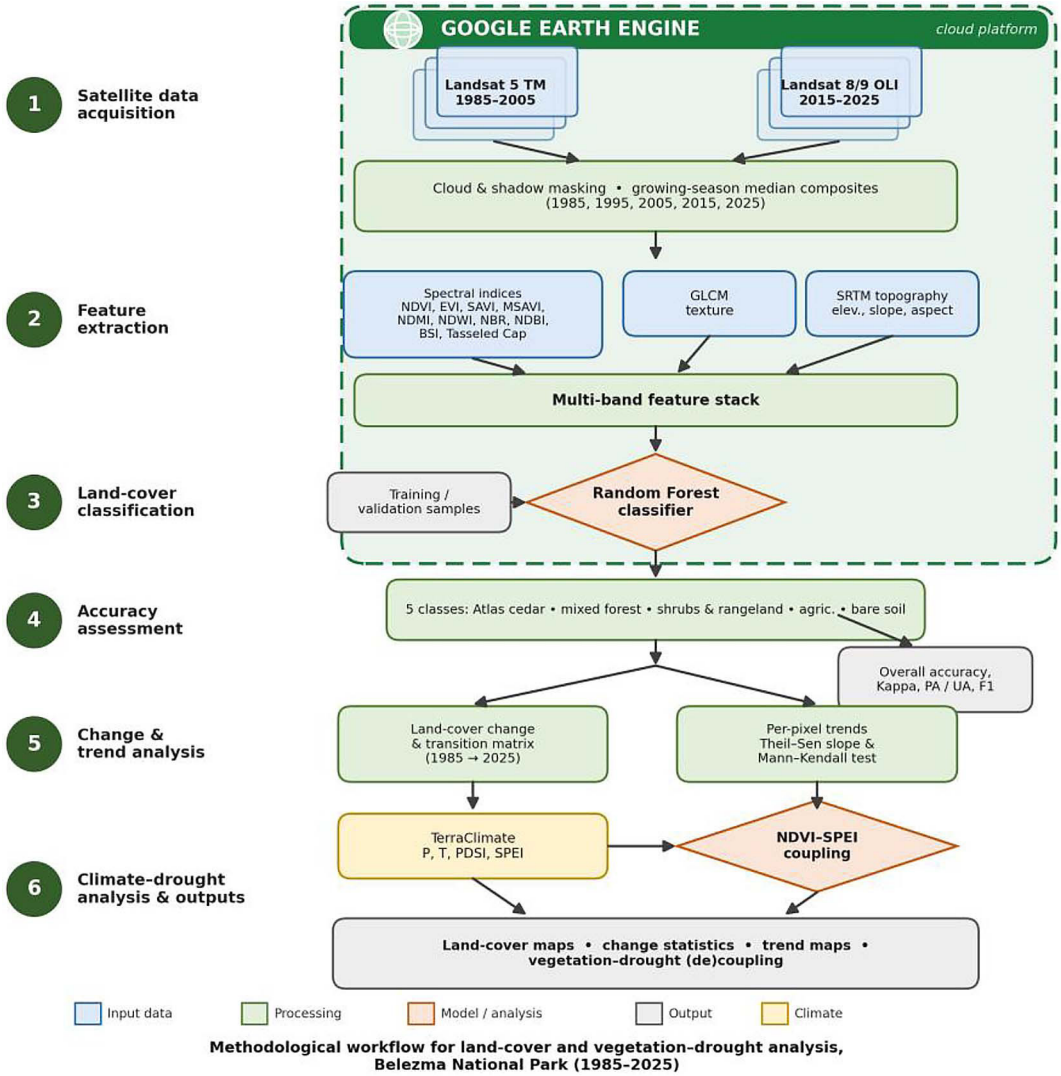

Figure 2. Methodological workflow for land-cover and vegetation–drought analysis of Belezma National Park (1985–2025), implemented largely in Google Earth Engine

preserving the seasonal window in which cedar and its competitors are spectrally most separable. The complete list of Landsat scenes used, with acquisition dates, sensor and cloud cover for both the classification composites and the annual time series, is provided in the repository (see Data and Code Availability). In total, 435 Landsat scenes contributed to the classification composites and 1.226 to the annual growing-season time series.

From each composite we derived a suite of spectral indices spanning greenness, canopy structure, moisture and burn sensitivity: NDVI (Tucker 1979), EVI, SAVI and MSAVI (Huete 1988), GNDVI, NDWI, NDMI, NBR, NDBI and BSI, together with Tasseled Cap components. Grey-level co-occurrence (GLCM) texture measures and SRTM-derived topographic variables (elevation, slope, aspect) were added to the feature stack to help the classifier exploit the strong terrain control on vegetation in this landscape.

Classification and accuracy assessment

Land cover was mapped for 1985, 1995, 2005, 2015 and 2025 using a Random Forest classifier (Breiman, 2001), which has become a standard for medium-resolution land-cover work because of its tolerance of high-dimensional, correlated feature sets and its competitive accuracy (Belgiu and Drăguț, 2016), with recent work tuning its parameters specifically for Earth Engine land-cover mapping (Sun and Ongsomwang, 2023). Five classes were distinguished: Atlas cedar, mixed forest, shrubs and rangeland, agricultural land, and bare soil. Training and validation samples were split so that accuracy could be assessed on data withheld from training, and performance was summarised by the overall accuracy and the kappa coefficient (Congalton, 1991; Foody, 2002), with kappa strength interpreted following the conventional benchmarks of Landis and Koch (1977). Class areas were computed inside the park boundary within Earth Engine; these clipped figures are reported as the authoritative areas throughout. The Random Forest was configured with 300 trees, a bag fraction of 0.6, a minimum leaf population of 1, and the number of variables tried at each split left at the Earth Engine default of the square root of the 27 input predictors (mtry ≈ 5); a fixed random seed of 42 was set throughout to ensure exact reproducibility. Reference samples were digitised as polygons for each epoch and the extracted pixels (34,810 in total) were split 70/30 into training (24,424) and validation (10,386) subsets, with the validation subset withheld from training.

Trend analysis

Per-pixel temporal trends in NDVI, EVI, NDMI, NBR and NDDI were estimated over the full annual series using ordinary least-squares slope, the non-parametric Theil–Sen slope estimator (Sen, 1968) and the Mann–Kendall test for monotonic trend (Kendall 1975); pixels were treated as significant at $p < 0.05$. The same procedure was applied to the annual park-mean index series and to the climate variables. We report Sen's slope alongside the linear slope because the former is robust to outliers and to the heavy-tailed interannual variability typical of semi-arid systems, while recognising that the test for significance and the estimator of magnitude answer different questions and need not agree (Zhou et al., 2023).

Climate data and drought indices

Climate variables were taken from TerraClimate (Abatzoglou et al., 2018), a ~4 km monthly reconstruction of climate and climatic water balance. We extracted precipitation, mean temperature, the Palmer Drought Severity Index, and a growing-season Standardized Precipitation Evapotranspiration Index (Vicente-Serrano et al., 2010; Beguería et al., 2014), and tested the SPEI–vegetation relationship at the annual scale following the rationale that vegetation responds to drought at characteristic time-scales (Vicente-Serrano et al., 2013; Gouveia et al., 2017). Two caveats apply and are carried through the interpretation. First, TerraClimate's long-term trends are partly inherited from its parent datasets and should not be treated as an independent trend estimate; its value here is in characterising interannual variability and relative drought timing rather than in certifying a standalone climatic trend. Second, the SPEI used here is a z-score approximation of the water-balance anomaly rather than the classic log-logistic formulation, so absolute index values are indicative rather than exact. The coarse 4 km grid also means that only a few independent cells fall within the park, so climate trends are reported as region-wide summaries rather than mapped at a resolution the data cannot support.

RESULTS

Land-cover change, 1985–2025

The five classifications were accurate and internally consistent. Overall accuracy ranged from 0.971 (2025) to 0.998 (2015) and the kappa coefficient from 0.962 to 0.997 (Table 1), placing every epoch in the "almost perfect" agreement band of Landis and Koch (1977). The slightly lower 2025 figures coincide with the most fragmented, post-drought landscape and the recent Landsat 8/9 composite, but the difference is small. The per-class metrics tell a more pointed story (Figure 3). Four of the five classes were classified accurately and stably across all epochs, but the producer's accuracy of Atlas cedar—high and stable through 2015—fell sharply to 0.73 by 2025 while its user's accuracy stayed high (0.94–1.00). In other words, the classifier increasingly failed to find real cedar (rising omission error) even though pixels labelled cedar were almost always correct. That asymmetry is itself a symptom of the decline: as crowns thin and defoliate, cedar pixels become spectrally harder to separate from mixed forest, which is exactly the confusion examined in the change analysis below.

Table 1. Random forest classification accuracy (overall accuracy and kappa) per mapping year

Year	Overall accuracy	Kappa
1985	0.980	0.974
1995	0.978	0.972
2005	0.975	0.967
2015	0.998	0.997
2025	0.971	0.962

Land cover changed substantially over the four decades (Figures 4a–3c, Figure 5, Figure 6; Table 2). The Atlas cedar class contracted from 1561 ha in 1985 to 720 ha in 2025, a net loss of 841 ha or 53.9% of its initial extent, equivalent to an average decline of about 1.35% of the 1985 area per year (Table 3). The loss was monotonic across all five epochs rather than concentrated in a single step, falling to 1347 ha by 1995, 1029 ha by 2005 and 819 ha by 2015 (Figure 7). Mixed forest moved in the opposite direction, expanding from 4506 to 8717 ha (+93.4%), with most of the gain realised by 1995. Shrubs and rangeland, the largest single class in 1985 at 14,412 ha, fell to 8021 ha (−44.3%), while agricultural land and bare soil both increased (+79.4% and +19.6% respectively), the latter fluctuating between epochs in a way that tracks the wet and dry years of the record.

The transition analysis between the 1985 and 2025 maps clarifies where the cedar went (Figure 8; Tables 4 and 5). Of the cedar present in 1985, 48.5% persisted as cedar, 42.8% was reclassified as mixed forest, and 7.7% became bare soil; conversion to shrubs or cropland was negligible (each below 0.5%). The pixel-overlay totals differ slightly from the Earth Engine clipped areas because the overlay was restricted to a raster footprint mask rather than the exact park polygon, but the proportional pathways are unaffected. The cedar-to-mixed-forest pathway admits two readings; the cedar-to-bare-soil pathway, by contrast, is unambiguous canopy loss. Class-level gross gains, gross losses and persistence per class over the same interval are summarised in Table 6.

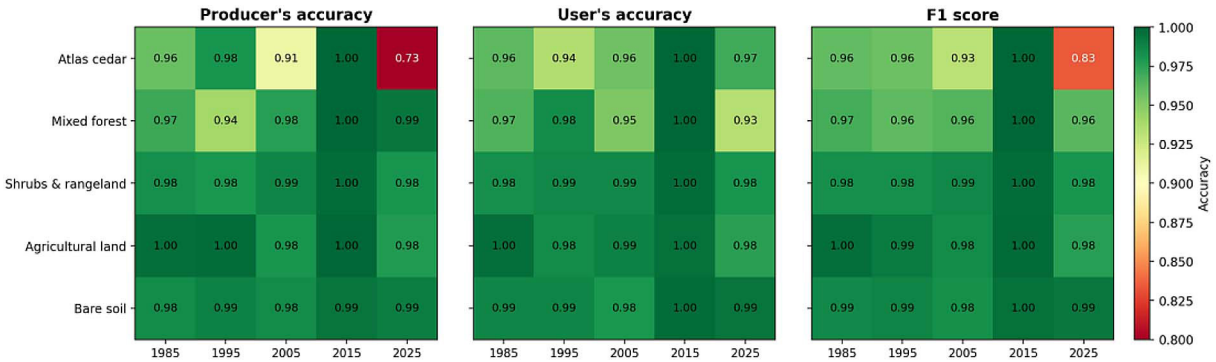

Figure 3. Per-class producer's accuracy, user's accuracy and F1 score by year, as annotated heatmaps (0.80–1.00 colour range)

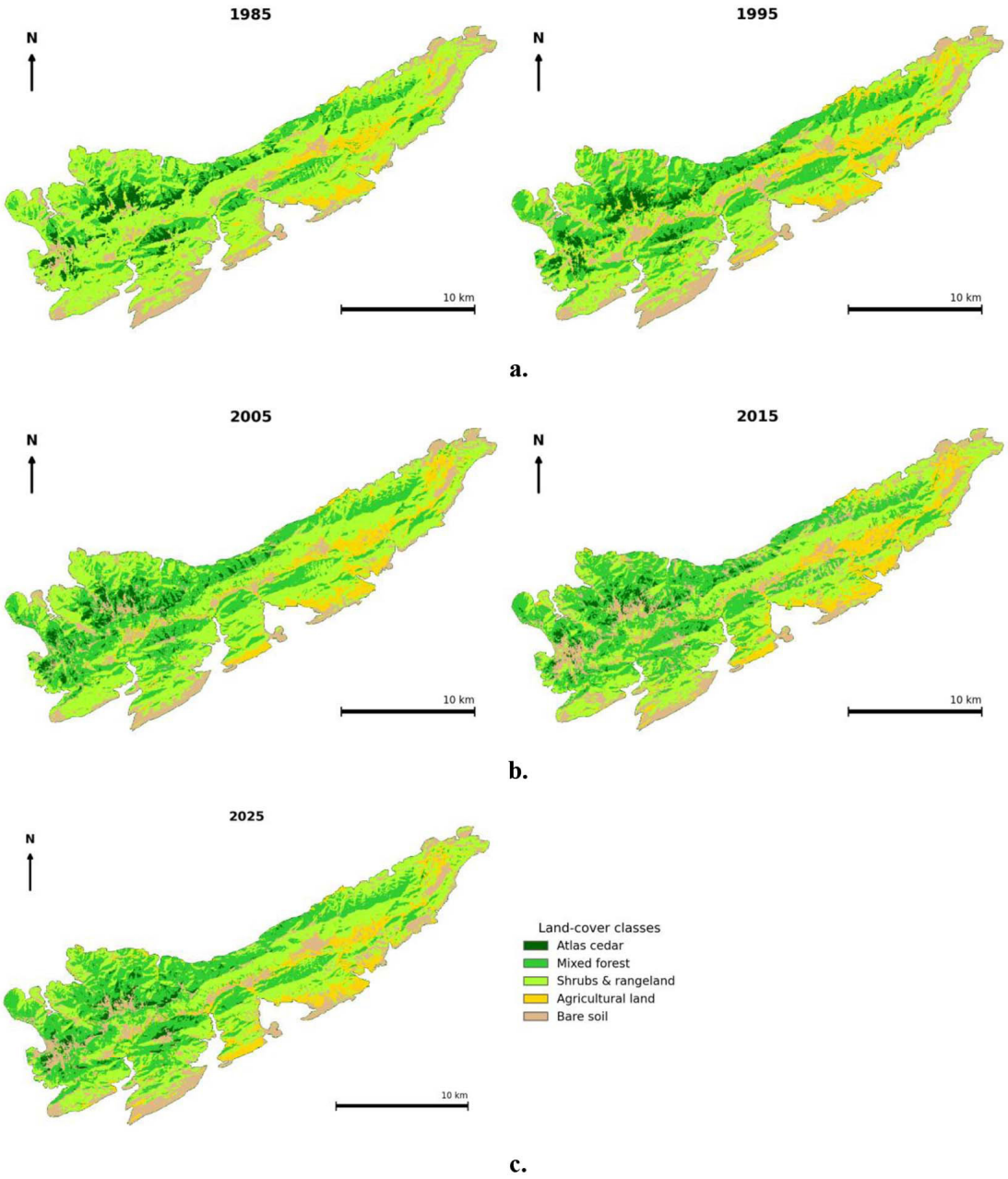

Figure 4. a. Random Forest land-cover classification of Belezma National Park for 1985 and 1995, b. Random Forest land-cover classification of Belezma National Park for 2005 and 2015, c. Random Forest land-cover classification of Belezma National Park for 2025, with the land-cover legend

Vegetation and moisture index trends

Park-mean greenness increased over the study period. NDVI rose at 0.0021 yr^{-1} (Sen's slope 0.0020 yr^{-1}; $R^2 = 0.31$; Mann–Kendall $p < 0.001$) and EVI at 0.0009 yr^{-1} ($p = 0.004$), both statistically significant increasing trends (Figure 9; Table 7). The moisture-sensitive NDMI and the burn-sensitive NBR showed weak positive slopes that were not significant ($p = 0.20$ and $p = 0.62$ respectively). The full annual series is punctuated by a pronounced trough around 2000–2002, visible in every index, that corresponds to the well-documented drought of that period. NDDI as exported contained division-by-near-zero artefacts spanning many orders of magnitude and was therefore excluded from the time-series analysis; its per-pixel trend layer is shown for completeness but not interpreted quantitatively. Spatially, the NDVI trend was predominantly positive across the park, with significant greening concentrated on the lower and mid-slope shrub and matorral zones (Figure 10). Embedded within this greening matrix are

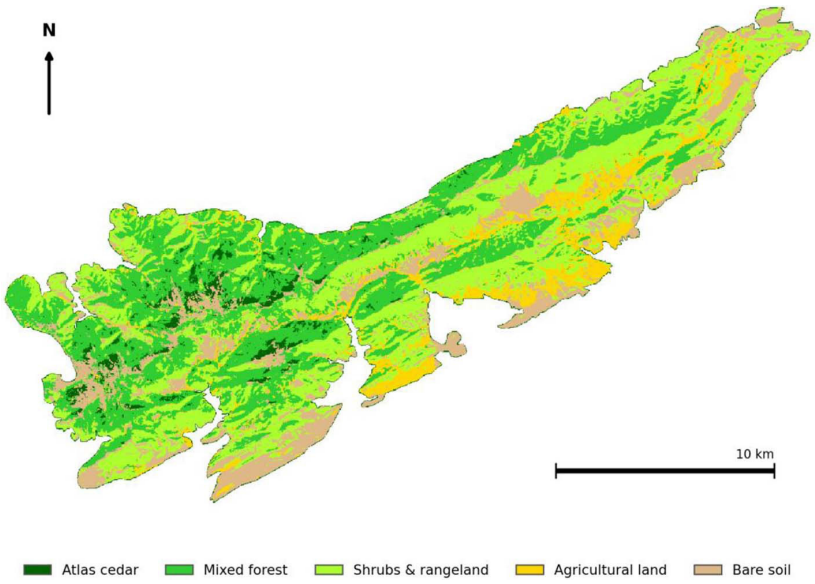

Figure 5. Most-recent (2025) land-cover map of Belezma National Park

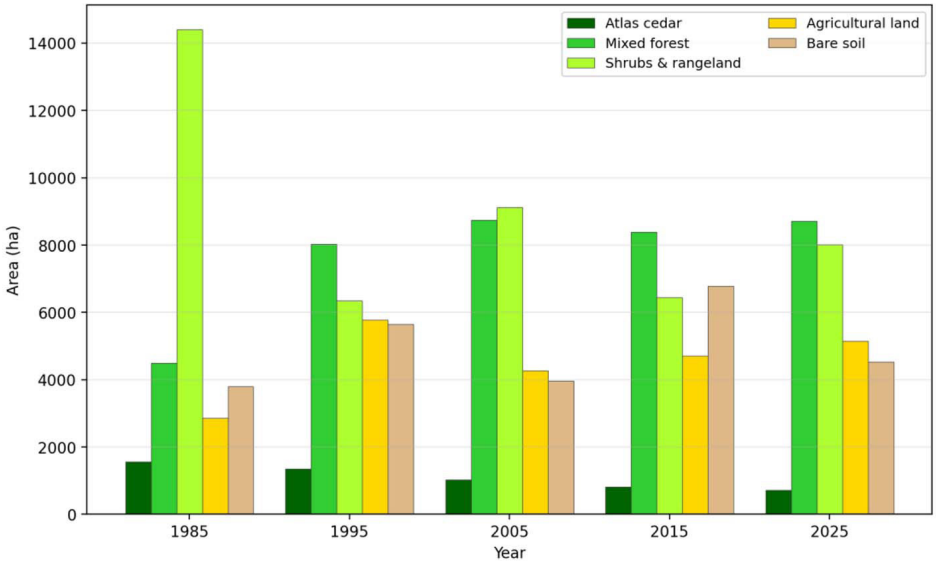

Figure 6. Land-cover area per class across the five mapping years

Table 2. Land-cover area per class (ha and % of park area), 1985–2025. Areas are computed inside the park boundary in Google Earth Engine

Land-cover class	1985	1995	2005	2015	2025
Atlas cedar	1561.3 (5.8%)	1347.1 (5.0%)	1029.0 (3.8%)	818.8 (3.0%)	719.8 (2.7%)
Mixed forest	4506.4 (16.6%)	8026.6 (29.6%)	8738.9 (32.2%)	8388.1 (30.9%)	8717.1 (32.1%)
Shrubs & rangeland	14411.6 (53.1%)	6352.7 (23.4%)	9127.4 (33.6%)	6438.7 (23.7%)	8021.3 (29.6%)
Agricultural land	2867.5 (10.6%)	5772.5 (21.3%)	4277.3 (15.8%)	4709.2 (17.4%)	5144.1 (19.0%)
Bare soil	3794.5 (14.0%)	5642.5 (20.8%)	3968.8 (14.6%)	6786.5 (25.0%)	4539.0 (16.7%)

discrete patches of significant negative NDVI slope on the upper slopes where cedar is concentrated, the spatial signature of localised canopy decline against a background of aggregate gain.

Climate trends and vegetation–drought coupling

The climate record over 1985–2024 is one of warming and drying (Figure 11; Table 7). Mean

Table 3. Net change, total percentage change and annual rate of change per land-cover class, 1985–2025

Land-cover class	1985 (ha)	2025 (ha)	Net change (ha)	Total change (%)	Annual rate (ha/yr)	Annual rate (%/yr)
Atlas cedar	1561.3	719.8	-841.4	-53.9	-21.0	-1.35
Mixed forest	4506.4	8717.1	4210.7	93.4	105.3	2.34
Shrubs & rangeland	14411.6	8021.3	-6390.3	-44.3	-159.8	-1.11
Agricultural land	2867.5	5144.1	2276.6	79.4	56.9	1.98
Bare soil	3794.5	4539.0	744.5	19.6	18.6	0.49

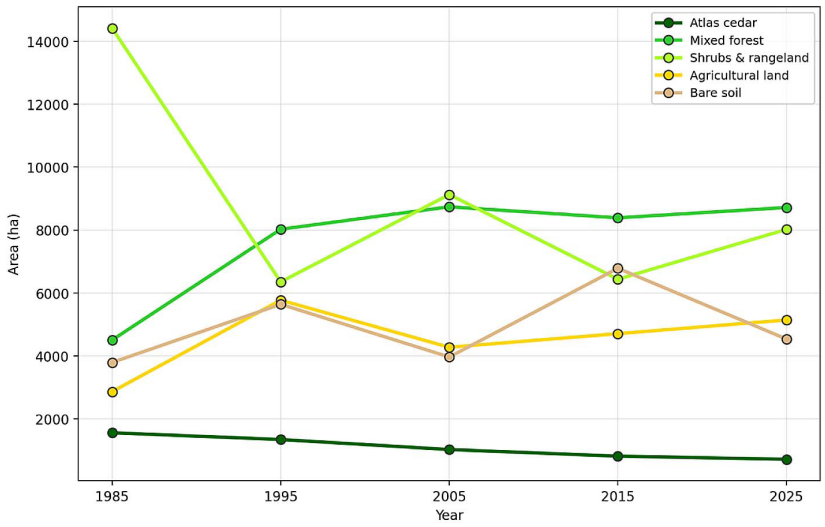

Figure 7. Trajectories of each land-cover class area over time, 1985–2025

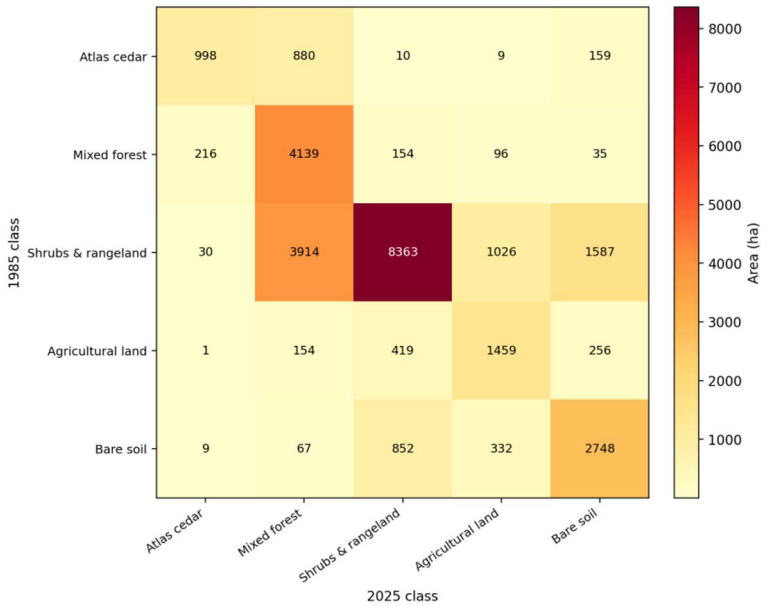

Figure 8. Heatmap of the 1985→2025 land-cover transition matrix (ha)

temperature increased significantly at 0.044 °C yr^{-1} ($p < 0.001$), about 1.7 °C across the four decades. Growing-season SPEI declined significantly (Sen's slope −0.039 yr^{-1}; Mann–Kendall $p = 0.017$) and PDSI fell in parallel ($p = 0.005$), both indicating a shift toward more frequent and more severe moisture deficit. Precipitation showed a negative slope (−6.4 mm $decade^{-1}$) that was not

Table 4. Land-cover transition matrix 1985→2025 (ha). Rows = 1985 class, columns = 2025 class. Totals reflect the raster footprint mask used for pixel overlay

From To	Atlas cedar	Mixed forest	Shrubs & rangeland	Agricultural land	Bare soil
Atlas cedar	998.0	880.5	9.6	8.8	159.0
Mixed forest	215.5	4138.7	153.7	95.6	34.9
Shrubs & rangeland	29.6	3913.6	8363.0	1026.4	1587.4
Agricultural land	0.8	154.3	419.1	1458.7	256.1
Bare soil	9.0	67.0	852.1	332.5	2747.7

Table 5. Fate of 1985 Atlas-cedar pixels by 2025

Cedar transitioned to	Area (ha)	% of 1985 cedar
Atlas cedar	998.0	48.5
Mixed forest	880.5	42.8
Shrubs & rangeland	9.6	0.5
Agricultural land	8.8	0.4
Bare soil	159.0	7.7

statistically significant, consistent with rainfall variability being high and the drying signal being driven as much by rising evaporative demand as by declining supply. Expressed as standardized trends per decade (Figure 12), every climate variable moved toward greater aridity: temperature rose by 0.43 °C decade^{-1} and both SPEI and PDSI fell significantly, while precipitation declined without reaching significance. This regional drying is in line with recent SPI/SPEI analyses of northern Algerian basins (Messis et al., 2025) and with projections of intensifying water stress for Mediterranean forest species (Enríquez-de-Salamanca, 2025).

The central result concerns the coupling between vegetation and drought. At the annual scale, park-mean NDVI was effectively uncorrelated

Table 6. Gross gains, gross losses and persistence by class, 1985–2025 (raster overlay)

Class	Area 1985 (ha)	Area 2025 (ha)	Persisted (ha)	Gross loss (ha)	Gross gain (ha)	Net change (ha)
Atlas cedar	2056.0	1253.0	998.0	1058.0	255.0	-803.0
Mixed forest	4638.5	9154.1	4138.7	499.8	5015.3	4515.6
Shrubs & rangeland	14919.9	9797.6	8363.0	6557.0	1434.6	-5122.4
Agricultural land	2289.0	2921.9	1458.7	830.3	1463.2	633.0
Bare soil	4008.3	4785.1	2747.7	1260.6	2037.4	776.8

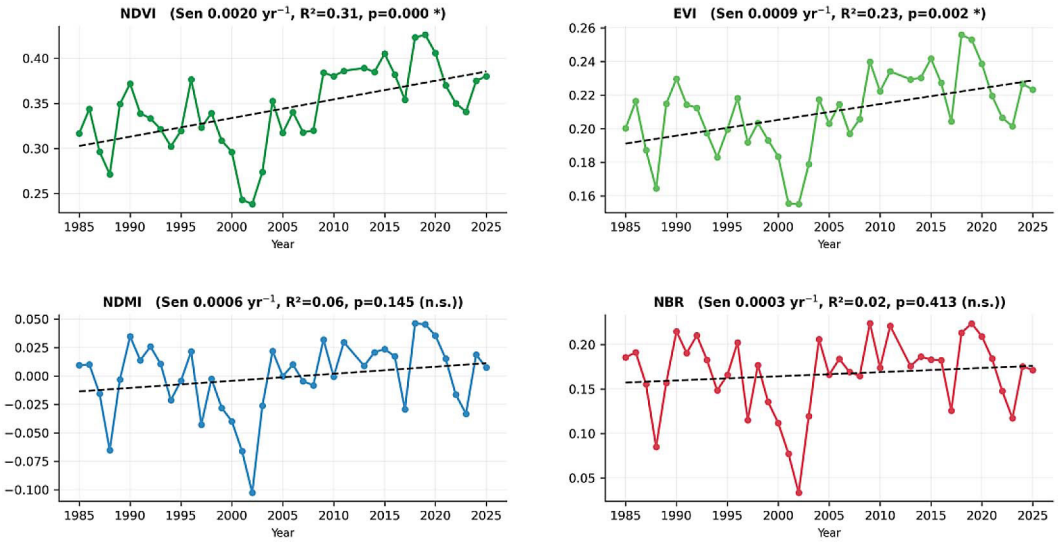

Figure 9. Annual mean vegetation and moisture indices (NDVI, EVI, NDMI, NBR) with linear and Sen's-slope trends

Table 7. Temporal trends (linear and Mann–Kendall / Sen's slope) of park-mean vegetation indices and climate variables, 1985–2024

Variable	Linear slope/yr	Sen slope/yr	R^2	Linear p	MK p	MK trend
NDVI	0.002	0.002	0.308	0	0	increasing
EVI	0.001	0.001	0.229	0.002	0.004	increasing
NDMI	0.001	0.001	0.055	0.145	0.204	no trend
NBR	0.001	0	0.018	0.413	0.616	no trend
pr	-0.686	-0.644	0.025	0.33	0.449	no trend
tmean	0.044	0.043	0.42	0	0	increasing
SPEI	-0.037	-0.039	0.184	0.006	0.017	decreasing
pdsi	-0.086	-0.092	0.169	0.009	0.005	decreasing

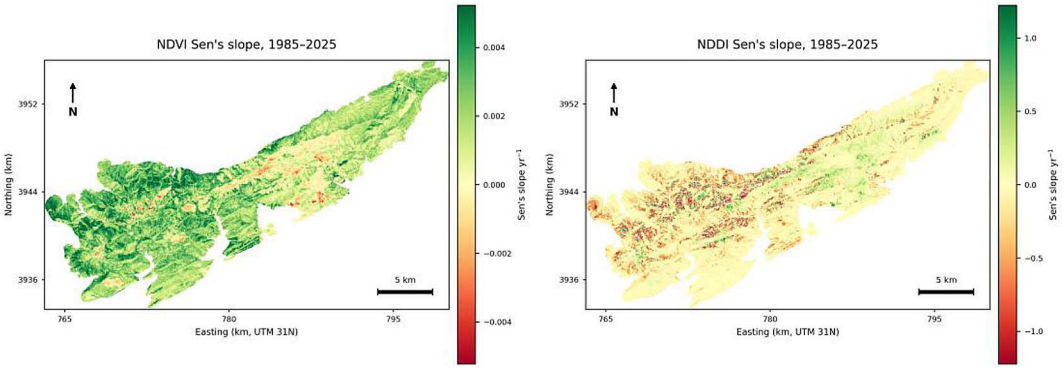

Figure 10. Per-pixel Sen's-slope trend maps of NDVI and NDDI; non-significant pixels (Mann–Kendall p ≥ 0.05) greyed

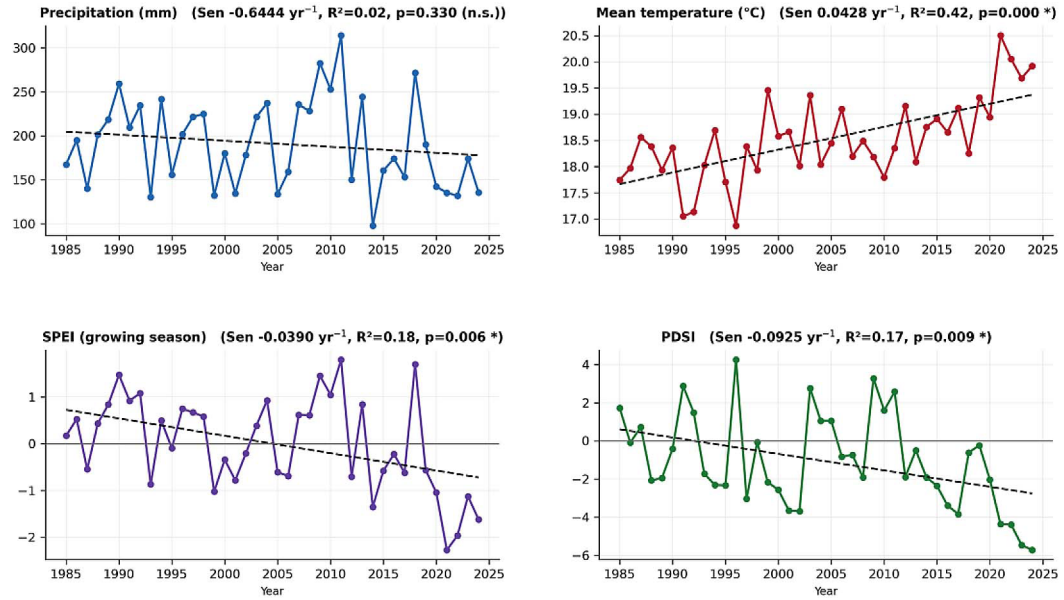

Figure 11. Annual climate variables (precipitation, mean temperature, SPEI, PDSI) with fitted trends

with growing-season SPEI (Pearson r = 0.09, p = 0.58, R^2 = 0.01, n = 39; Figure 13). The dual-axis series makes the divergence plain: NDVI climbs across the record while SPEI trends downward, and the recent run of strongly negative SPEI years after 2018 is not matched by any comparable decline in greenness (Figure 14). Vegetation activity at the scale of the whole park is therefore

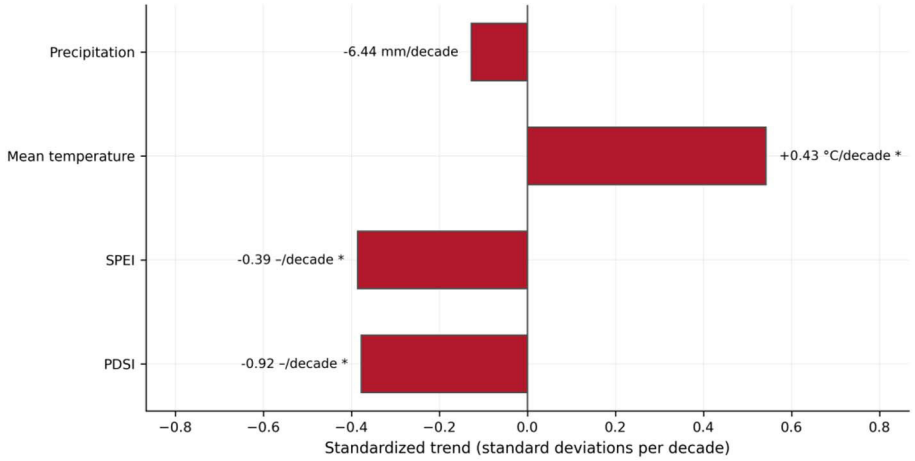

Figure 12. Standardized trends (standard deviations per decade) of precipitation, mean temperature, SPEI and PDSI from TerraClimate, with native-unit change per decade; * marks Mann–Kendall significance at $p < 0.05$

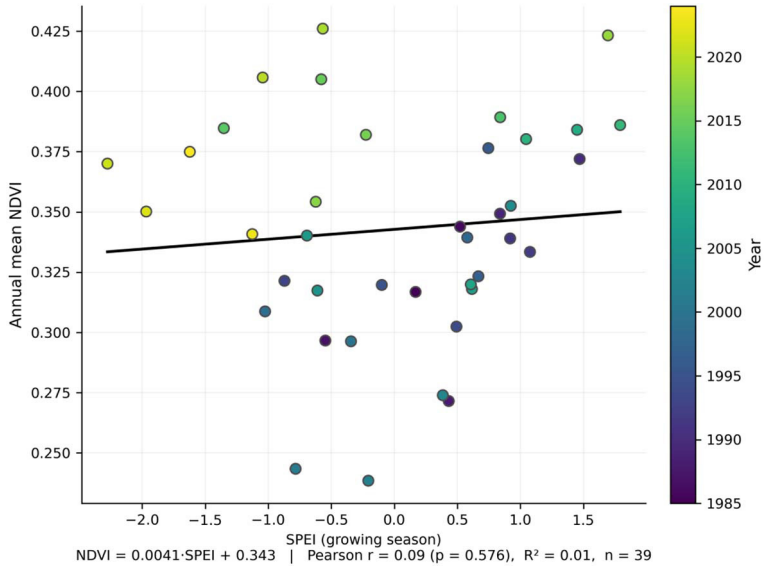

Figure 13. Annual NDVI against growing-season SPEI with OLS fit, Pearson r and R^2

decoupled from the climatic drought signal that, on independent grounds, is intensifying.

DISCUSSION

The two headline findings of this study pull in opposite directions and have to be reconciled: the park is getting greener on average, yet its keystone conifer has lost roughly half of its mapped area, and aggregate greenness is indifferent to a drought signal that is clearly strengthening. The reconciliation lies in scale and composition. Cedar occupied under 1.600 ha in 1985, less than 6% of the park, and now occupies under 800 ha. A loss of that magnitude is ecologically dramatic but areally small, and it is readily swamped in a park-mean NDVI by the much larger shrub, rangeland and mixed-forest matrix that has been filling in and intensifying. The transition matrix shows exactly this redistribution: large exchanges between shrubland and mixed forest, with shrubs and rangeland converting substantially to mixed forest, which raises mean greenness even as cedar disappears beneath it. Aggregate greening, in other words, is not evidence of ecosystem health; it is the statistical shadow of a few large, comparatively drought-tolerant classes expanding while a small, drought-sensitive one collapses.

The decoupling of park-mean NDVI from SPEI should be read in that light rather than as evidence that drought is irrelevant. A whole-park average mixes pixels with opposite responses: drought-tolerant shrub and matorral that green

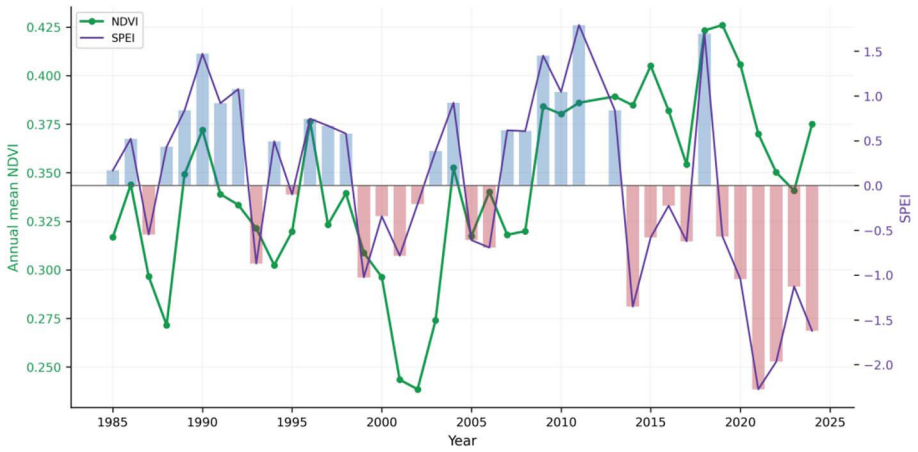

Figure 14. Dual-axis time series of annual NDVI and growing-season SPEI

up with CO_2 enrichment, land-use relaxation and the recovery of cool-season growth, set against drought-stressed cedar that browns and dies. The climatic signal cancels in the mean. This is consistent with the established understanding that vegetation responds to drought at class- and timescale-specific lags rather than uniformly (Vicente-Serrano et al., 2013; Gouveia et al., 2017); the discrete negative-NDVI patches on the upper slopes (Figure 10) track the loss far better than any park-wide mean.

That cedar decline is real and severe is not in doubt, and our magnitude, about 54% area loss over forty years, sits alongside earlier Aurès and Belezma assessments of multi-decadal cedar retreat (Belloula and Beghami, 2018; Ait Medjber et al., 2024). The climatic context we recover, significant warming of roughly 1.7 °C and a significant decline in SPEI and PDSI, matches the regional picture of intensifying Mediterranean drought (Hoerling et al., 2012) and the long-term aridification inferred from tree rings across northwestern Africa (Touchan et al., 2011; Cook et al., 2016). It also aligns with the dendrochronological attribution of Algerian cedar decline to a shift toward drier conditions (Sarmoum et al., 2019) and with the age-dependent drought sensitivity documented in the Moroccan Middle Atlas (Linares et al., 2011; Linares et al., 2013). Because Algerian cedar growth and phenology track cool-season precipitation closely (Missaoui et al., 2020; Slimani et al., 2021), the multi-decadal decline in SPEI we recover is a plausible chronic stressor. Drought is the slow-acting predisposing stress.

But the weak interannual SPEI–NDVI coupling, and the timing of the steepest cedar losses, argue against a purely climatic account. The largest decadal drop in cedar area straddles the 1995–2005 window, which contains the severe turn-of-the-century drought, yet the subsequent losses continued through periods that were not exceptionally dry. This is the pattern that would be expected if drought predisposes trees that are subsequently killed by biotic agents, consistent with reports that bark beetle and wood-borer outbreaks have contributed to cedar mortality in the Aurès (Beghami et al., 2020), set within the rich and still-emerging arthropod fauna of Belezma (Zereg et al., 2025). Grazing, fuelwood extraction and fire, all chronic pressures in a park embedded in a populated countryside, may further erode regeneration and are consistent with the conversion of dying stands to bare soil, the pathway that accounts for the unambiguous 8% of 1985 cedar now mapped as bare ground. Cedar decline at Belezma is therefore most plausibly interpreted as drought-predisposed and disturbance-precipitated, a compound process in which climate is likely to set the stage while insects, livestock and people act as probable proximate agents, an interpretation our data are consistent with but cannot, on their own, establish. Independent field photographs taken within the park document standing dead cedar snags, defoliated crowns and thinning upper-slope canopy (see Data and Code Availability), providing ground-based corroboration of this mortality from our own observations rather than the literature alone.

Several limitations bound these conclusions. The cedar-to-mixed-forest transition cannot be fully partitioned between true compositional replacement and spectral reclassification of defoliated cedar canopies, and field validation of the

upper-slope decline patches would sharpen that distinction. The class areas carry the usual medium-resolution uncertainty even at the high accuracies achieved. The climate analysis rests on a 4 km product whose long-term trends are partly inherited and whose grid resolves the park into only a handful of cells, so the climatic trends are regionally reliable but spatially coarse, and the SPEI is an approximation. None of these caveats overturns the central narrative, but each marks where the evidence is strongest and where it is merely indicative. Finally, although our classification, the cedar-to-bare-soil pathway and the field photographs together confirm real cedar mortality, the relative contributions of drought, insect outbreaks and anthropogenic pressure cannot be quantitatively partitioned from the present data; that attribution is inferred partly from the regional literature and would require targeted entomological and dendrochronological field surveys to resolve.

For management, the practical message is that Belezma's cedar requires targeted intervention that a park-scale greenness metric will neither detect nor reward. Protecting the surviving upper-slope stands, controlling grazing and fuelwood pressure in and around them, monitoring for bark-beetle activity, and assisting regeneration in the cedar-to-bare-soil conversion zones are actions aimed at the actual locus of loss. Distribution models that project upslope range contraction under continued warming (Laala and Adimi, 2024) reinforce the case for prioritising the highest and coolest refugia. Continued greening of the surrounding matorral is not a substitute for, and should not be mistaken for, the persistence of the species the park was created to protect.

CONCLUSIONS

Over 1985–2025, Belezma National Park became greener on average while losing roughly half of its Atlas cedar cover. The contradiction resolves through scale: a small, drought-sensitive keystone is collapsing beneath an expanding shrub and mixed-forest matrix, so park-mean NDVI rises and remains uncorrelated with a regional climate that is significantly warming and drying. The loss is most plausibly drought-predisposed and disturbance-driven, with bark-beetle outbreaks, grazing and fire as likely proximate agents whose relative roles remain to be quantified by targeted field survey. Detecting and reversing it requires stand-level monitoring rather than park-wide vegetation indices, which here give a misleadingly reassuring signal.

Data and code availability

All code, data and materials supporting this study are openly available at <REPOSITORY_URL> (archived at <DOI>). The archive contains the complete Google Earth Engine script; the classified land-cover maps for 1985–2025 (GeoTIFF, EPSG:32631, 30 m; class codes 0–4, 255 = NoData); the full training and validation dataset (377 training polygons in Shapefile and GeoJSON, and 34,810 extracted per-pixel samples with all 27 predictors, class label, train/test split and year); the per-class sample counts, per-class accuracies and full confusion matrices; the vegetation- and climate-index time-series tables and the Theil–Sen and Mann–Kendall trend rasters; the explicit list of Landsat scenes used (435 for the classification composites, 1,226 for the annual time series); and geolocated field photographs documenting cedar mortality. The Random Forest classifier used 300 trees, a bag fraction of 0.6, the default mtry ($\sqrt{27}$) and a fixed seed of 42.

REFERENCES

1. Abatzoglou, J.T., Dobrowski, S.Z., Parks, S.A., Hegewisch, K.C. (2018). TerraClimate, a high-resolution global dataset of monthly climate and climatic water balance from 1958–2015. *Scientific Data*, *5*, 170191. https://doi.org/10.1038/sdata.2017.191
2. Abdessemed, K. (1981). *Le cèdre de l'Atlas (Cedrus atlantica Manetti) dans le massif des Aurès et de Bélezma: Étude phytosociologique, problèmes de conservation et d'aménagement* [PhD dissertation]. Université d'Aix-Marseille, France.
3. Ait Medjber, R., Ben Messaoud, H., Soualah, H.A. (2024). Multispectral satellite datasets for detection and mapping of land cover change in a Mediterranean area of North Africa, Belezma (Algeria). *Environmental Research, Engineering and Management*, *80*(1), 39–49. https://doi.org/10.5755/j01.erem.80.1.32704
4. Alba-Sánchez, F., Abel-Schaad, D., Iriarte, E., López-Sáez, J.A., Cheddadi, R., Pérez-Díaz, S., González-Hernández, A. (2025a). Postglacial dynamics of Cedrus atlantica in North African montane forests: A paleoecological perspective on a Mediterranean conifer. *Quaternary Science Reviews*, *370*, 109633. https://doi.org/10.1016/j.

quascirev.2025.109633

5. Alba-Sánchez, F., Abel-Schaad, D., López-Sáez, J.A., Romera-Romera, D., Pérez-Díaz, S., González-Hernández, A. (2025b). Seven millennia of Cedrus atlantica forest dynamics in the Western Rif Mountains (Morocco). *Forests*, *16*(9), 1441. https://doi.org/10.3390/f16091441
6. Beghami, R., Bertella, N., Laamari, M., Bensaci, O.A. (2020). Bark beetle and wood-borer insects' outbreak as a potent driver of Atlas cedar (Cedrus atlantica (Endl.) Carrière) forests dieback in Aurès – East Algeria. *Forest Science and Technology*, *16*(2), 75–85. https://doi.org/10.1080/21580103.2020.1756929
7. Beguería, S., Vicente-Serrano, S.M., Reig, F., Latorre, B. (2014). Standardized precipitation evapotranspiration index (SPEI) revisited. *International Journal of Climatology*, *34*(10), 3001–3023. https://doi.org/10.1002/joc.3887
8. Belgiu, M., Drăguț, L. (2016). Random forest in remote sensing: A review of applications and future directions. *ISPRS Journal of Photogrammetry and Remote Sensing*, *114*, 24–31. https://doi.org/10.1016/j.isprsjprs.2016.01.011
9. Belloula, S., Beghami, Y. (2018). Assessment of the dynamics of Atlas cedar decline (*Cedrus atlantica* Manetti) by remote sensing in the Aurès area, Algeria. *Arab World Geographer 21.*
10. Bentouati, A. (2008). La situation du cèdre de l'Atlas en Algérie. *Forêt Méditerranéenne*, *29*(2), 203–208.
11. Bentouati, A., Bariteau, M. (2006). Réflexion sur le dépérissement du cèdre de l'Atlas des Aurès (Algérie). *Forêt Méditerranéenne*, *27*(4), 317–322.
12. Bouahmed, A., Vessella, F., Schirone, B., Krouchi, F., Derridj, A. (2019). Modeling *Cedrus atlantica* potential distribution in North Africa across time: New putative glacial refugia and future range shifts under climate change. *Regional Environmental Change*, *19*(6), 1667–1682. https://doi.org/10.1007/s10113-019-01503-w
13. Breiman, L. (2001). Random forests. *Machine Learning*, *45*(1), 5–32. https://doi.org/10.1023/A:1010933404324
14. Cedrus atlantica — Threatened conifers of the world. (n.d.). Royal Botanic Garden Edinburgh. https://threatenedconifers.rbge.org.uk/conifers/cedrus-atlantica
15. Congalton, R.G. (1991). A review of assessing the accuracy of classifications of remotely sensed data. *Remote Sensing of Environment*, *37*(1), 35–46. https://doi.org/10.1016/0034-4257(91)90048-B
16. Cook, B.I., Anchukaitis, K.J., Touchan, R., Meko, D.M., Cook, E.R. (2016). Spatiotemporal drought variability in the Mediterranean over the last 900 years. *Journal of Geophysical Research: Atmospheres*, *121*(5), 2060–2074. https://doi.org/10.1002/2015JD023929
17. Enríquez-de-Salamanca, Á. (2025). Expected impacts on Mediterranean forest species under climate change. *Climate*, *13*(2), 41. https://doi.org/10.3390/cli13020041
18. Esper, J., et al. (2024). Dendrochronological studies in North Africa: Reality and prospects. *Frontiers in Ecology and Evolution*, *12*, 1299472. https://doi.org/10.3389/fevo.2024.1299472
19. Foody, G.M. (2002). Status of land cover classification accuracy assessment. *Remote Sensing of Environment*, *80*(1), 185–201. https://doi.org/10.1016/S0034-4257(01)00295-4
20. Gorelick, N., Hancher, M., Dixon, M., Ilyushchenko, S., Thau, D., Moore, R. (2017). Google Earth Engine: Planetary-scale geospatial analysis for everyone. *Remote Sensing of Environment*, *202*, 18–27. https://doi.org/10.1016/j.rse.2017.06.031
21. Gouveia, C.M., Trigo, R.M., Beguería, S., Vicente-Serrano, S.M. (2017). Drought impacts on vegetation activity in the Mediterranean region: An assessment using remote sensing data and multi-scale drought indicators. *Global and Planetary Change*, *151*, 15–27. https://doi.org/10.1016/j.gloplacha.2016.06.011
22. Habibi, B., Meddi, M., Torfs, P.J.J.F., Remaoun, M., Van Lanen, H.A.J. (2018). Characterisation and prediction of meteorological drought using stochastic models in the semi-arid Chéliff–Zahrez basin (Algeria). *Journal of Hydrology: Regional Studies*, *16*, 15–31. https://doi.org/10.1016/j.ejrh.2018.02.005
23. Hoerling, M., Eischeid, J., Perlwitz, J., et al. (2012). On the increased frequency of Mediterranean drought. *Journal of Climate*, *25*(6), 2146–2161. https://doi.org/10.1175/JCLI-D-11-00296.1
24. Huete, A.R. (1988). A soil-adjusted vegetation index (SAVI). *Remote Sensing of Environment*, *25*(3), 295–309. https://doi.org/10.1016/0034-4257(88)90106-X
25. Kendall, M.G. (1975). *Rank correlation methods* (4th ed.). Charles Griffin.
26. Khenioui, A., Boukhalfa, S., Bougherara, A. (2023). The use of remote sensing and Geographic Information Systems in monitoring drought in the Algerian steppe. *Technium Social Sciences Journal*, *39*(1), 644–658. https://doi.org/10.47577/tssj.v39i1.7955
27. Kherchouche, D., Kalla, M., Gutiérrez, E., et al. (2012). Impact of droughts on Cedrus atlantica forests dieback in the Aurès (Algeria). *Journal of Life Sciences*, *6*, 1262–1269.
28. Laala, A., Adimi, A. (2024). Modeling the potential distribution and shift of an Algerian endangered endemic species (*Cedrus atlantica*) under climate change scenarios: Implications for conservation. *Journal for Nature Conservation*, *82*, 126744. https://doi.org/10.1016/j.jnc.2024.126744
29. Landis, J.R., Koch, G.G. (1977). The measurement of

observer agreement for categorical data. *Biometrics*, *33*(1), 159–174. https://doi.org/10.2307/2529310

30. Linares, J.C., Taïqui, L., Camarero, J.J. (2011). Increasing drought sensitivity and decline of Atlas cedar (*Cedrus atlantica*) in the Moroccan Middle Atlas forests. *Forests*, *2*(3), 777–796. https://doi.org/10.3390/f2030777
31. Linares, J.C., Taïqui, L., Sangüesa-Barreda, G., Seco, J.I., Camarero, J.J. (2013). Age-related drought sensitivity of Atlas cedar (*Cedrus atlantica*) in the Moroccan Middle Atlas forest. *Dendrochronologia*, *31*(2), 88–96. https://doi.org/10.1016/j.dendro.2012.08.003
32. Messis, M.-S., Kubiak-Wójcicka, K., Mebarki, A., Merabti, A. (2025). Spatio-temporal meteorological drought distribution in the Upper Cheliff Basin (Algeria) using SPI and SPEI indices. *Climate*, *13*(6), 123. https://doi.org/10.3390/cli13060123
33. Missaoui, K., Gharzouli, R., Djellouli, Y., Messner, F. (2020). Phenological behavior of Atlas cedar (*Cedrus atlantica*) forest to snow and precipitation variability in Boutaleb and Babors Mountains, Algeria. *Biodiversitas*, *21*(1), 239–245. https://doi.org/10.13057/biodiv/d210131
34. Sarmoum, M., Navarro-Cerrillo, R.M., et al. (2019). The decline of Algerian Cedrus atlantica forests is driven by a climate shift towards drier conditions. *Dendrochronologia*, *55*, 60–70. https://doi.org/10.1016/j.dendro.2019.03.004
35. Sen, P.K. (1968). Estimates of the regression coefficient based on Kendall's tau. *Journal of the American Statistical Association*, *63*(324), 1379–1389. https://doi.org/10.1080/01621459.1968.10480934
36. Slimani, S., Kherchouche, D., Bekdouche, F., Gutiérrez, E. (2021). Tree-ring reconstruction of March–June precipitation from the Atlas cedar forest of Mount Takoucht, Béjaïa (northern Algeria). *Forest Systems*, *30*(3), e011. https://doi.org/10.5424/fs/2021303-18111
37. Sun, J., Ongsomwang, S. (2023). Optimal parameters of random forest for land cover classification with suitable data type and dataset on Google Earth Engine. *Frontiers in Earth Science*, *11*, 1188093. https://doi.org/10.3389/feart.2023.1188093
38. Touchan, R., Anchukaitis, K.J., Meko, D.M., et al. (2011). Spatiotemporal drought variability in northwestern Africa over the last nine centuries. *Climate Dynamics*, *37*, 237–252. https://doi.org/10.1007/s00382-010-0804-4
39. Tucker, C.J. (1979). Red and photographic infrared linear combinations for monitoring vegetation. *Remote Sensing of Environment*, *8*(2), 127–150. https://doi.org/10.1016/0034-4257(79)90013-0
40. Vicente-Serrano, S.M., Beguería, S., López-Moreno, J.I. (2010). A multiscalar drought index sensitive to global warming: The Standardized Precipitation Evapotranspiration Index (SPEI). *Journal of Climate*, *23*(7), 1696–1718. https://doi.org/10.1175/2009JCLI2909.1
41. Vicente-Serrano, S.M., Gouveia, C., Camarero, J.J., et al. (2013). Response of vegetation to drought time-scales across global land biomes. *Proceedings of the National Academy of Sciences*, *110*(1), 52–57. https://doi.org/10.1073/pnas.1207068110
42. Zereg, S., Mouane, A., Aouadi, A. (2025). Diversity and spatio-temporal distribution of arthropods in the Atlas cedar (Cedrus atlantica Manetti) forest in Belezma National Park (Batna, Algeria). *Journal of Insect Biodiversity and Systematics*, *11*(1), 97–115. https://doi.org/10.61186/jibs.11.1.97
43. Zhou, J., Deitch, M.J., Grunwald, S., Screaton, E. (2023). Do the Mann-Kendall test and Theil-Sen slope fail to inform trend significance and magnitude in hydrology? *Hydrological Sciences Journal*, *68*(9), 1241–1249. https://doi.org/10.1080/02626667.2023.2212166